Transverse and Longitudinal Bose-Einstein Correlations in Hadronic Z^0 Decays

The OPAL Collaboration

Abstract

Bose-Einstein correlations in pairs of identical charged pions produced in a sample of 4.3 million Z^0 hadronic decays are studied as a function of the three components of the momentum difference, transverse ("out" and "side") and longitudinal with respect to the thrust direction of the event. A significant difference between the transverse, $r_{t_{side}}$, and longitudinal, r_l, dimensions is observed, indicating that the emitting source of identical pions, as observed in the Longitudinally CoMoving System, has an elongated shape. This is observed with a variety of selection techniques. Specifically, the values of the parameters obtained by fitting the extended Goldhaber parametrisation to the correlation function $C' = C^{\mathrm{DATA}}/C^{\mathrm{MC}}$ for two-jet events, selected with the Durham algorithm and resolution parameter $y_{cut} = 0.04$, are $r_{t_{side}} = (0.809 \pm 0.009 \ (stat) \ ^{+0.019}_{-0.032} \ (syst))$ fm, $r_l = (0.989 \pm 0.011 \ (stat) \ ^{+0.030}_{-0.015} \ (syst))$ fm and $r_l/r_{t_{side}} = 1.222 \pm 0.027 \ (stat) \ ^{+0.075}_{-0.012} \ (syst)$. The results are discussed in the context of a recent model of Bose-Einstein correlations based on string fragmentation.

The OPAL Collaboration

G. Abbiendi[2], K. Ackerstaff[8], P.F. Akesson[3], G. Alexander[22], J. Allison[16], K.J. Anderson[9], S. Arcelli[17], S. Asai[23], S.F. Ashby[1], D. Axen[27], G. Azuelos[18,a], I. Bailey[26], A.H. Ball[8], E. Barberio[8], R.J. Barlow[16], J.R. Batley[5], S. Baumann[3], T. Behnke[25], K.W. Bell[20], G. Bella[22], A. Bellerive[9], S. Bentvelsen[8], S. Bethke[14,i], O. Biebel[14,i], A. Biguzzi[5], I.J. Bloodworth[1], P. Bock[11], J. Böhme[14,h], O. Boeriu[10], D. Bonacorsi[2], M. Boutemeur[31], S. Braibant[8], P. Bright-Thomas[1], L. Brigliadori[2], R.M. Brown[20], H.J. Burckhart[8], J. Cammin[3], P. Capiluppi[2], R.K. Carnegie[6], A.A. Carter[13], J.R. Carter[5], C.Y. Chang[17], D.G. Charlton[1,b], D. Chrisman[4], C. Ciocca[2], P.E.L. Clarke[15], E. Clay[15], I. Cohen[22], O.C. Cooke[8], J. Couchman[15], C. Couyoumtzelis[13], R.L. Coxe[9], M. Cuffiani[2], S. Dado[21], G.M. Dallavalle[2], S. Dallison[16], R. Davis[28], A. de Roeck[8], P. Dervan[15], K. Desch[25], B. Dienes[30,h], M.S. Dixit[7], M. Donkers[6], J. Dubbert[31], E. Duchovni[24], G. Duckeck[31], I.P. Duerdoth[16], P.G. Estabrooks[6], E. Etzion[22], F. Fabbri[2], A. Fanfani[2], M. Fanti[2], A.A. Faust[28], L. Feld[10], P. Ferrari[12], F. Fiedler[25], M. Fierro[2], I. Fleck[10], A. Frey[8], A. Fürtjes[8], D.I. Futyan[16], P. Gagnon[12], J.W. Gary[4], G. Gaycken[25], C. Geich-Gimbel[3], G. Giacomelli[2], P. Giacomelli[2], D.M. Gingrich[28,a], D. Glenzinski[9], J. Goldberg[21], W. Gorn[4], C. Grandi[2], K. Graham[26], E. Gross[24], J. Grunhaus[22], M. Gruwé[25], P.O. Günther[3], C. Hajdu[29] G.G. Hanson[12], M. Hansroul[8], M. Hapke[13], K. Harder[25], A. Harel[21], C.K. Hargrove[7], M. Harin-Dirac[4], A. Hauke[3], M. Hauschild[8], C.M. Hawkes[1], R. Hawkings[25], R.J. Hemingway[6], C. Hensel[25], G. Herten[10], R.D. Heuer[25], M.D. Hildreth[8], J.C. Hill[5], P.R. Hobson[25], A. Hocker[9], K. Hoffman[8], R.J. Homer[1], A.K. Honma[8], D. Horváth[29,c], K.R. Hossain[28], R. Howard[27], P. Hüntemeyer[25], P. Igo-Kemenes[11], D.C. Imrie[25], K. Ishii[23], F.R. Jacob[20], A. Jawahery[17], H. Jeremie[18], M. Jimack[1], C.R. Jones[5], P. Jovanovic[1], T.R. Junk[6], N. Kanaya[23], J. Kanzaki[23], G. Karapetian[18], D. Karlen[6], V. Kartvelishvili[16], K. Kawagoe[23], T. Kawamoto[23], P.I. Kayal[28], R.K. Keeler[26], R.G. Kellogg[17], B.W. Kennedy[20], D.H. Kim[19], K. Klein[11], A. Klier[24], T. Kobayashi[23], M. Kobel[3], T.P. Kokott[3], M. Kolrep[10], S. Komamiya[23], R.V. Kowalewski[26], T. Kress[4], P. Krieger[6], J. von Krogh[11], T. Kuhl[3], M. Kupper[24], P. Kyberd[13], G.D. Lafferty[16], H. Landsman[21], D. Lanske[14], I. Lawson[26], J.G. Layter[4], A. Leins[31], D. Lellouch[24], J. Letts[12], L. Levinson[24], R. Liebisch[11], J. Lillich[10], B. List[8], C. Littlewood[5], A.W. Lloyd[1], S.L. Lloyd[13], F.K. Loebinger[16], G.D. Long[26], M.J. Losty[7], J. Lu[27], J. Ludwig[10], A. Macchiolo[18], A. Macpherson[28], W. Mader[3], M. Mannelli[8], S. Marcellini[2], T.E. Marchant[16], A.J. Martin[13], J.P. Martin[18], G. Martinez[17], T. Mashimo[23], P. Mättig[24], W.J. McDonald[28], J. McKenna[27], T.J. McMahon[1], R.A. McPherson[26], F. Meijers[8], P. Mendez-Lorenzo[31], F.S. Merritt[9], H. Mes[7], I. Meyer[5], A. Michelini[2], S. Mihara[23], G. Mikenberg[24], D.J. Miller[15], W. Mohr[10], A. Montanari[2], T. Mori[23], K. Nagai[8], I. Nakamura[23], H.A. Neal[12,f], R. Nisius[8], S.W. O'Neale[1], F.G. Oakham[7], F. Odorici[2], H.O. Ogren[12], A. Okpara[11], M.J. Oreglia[9], S. Orito[23], G. Pásztor[29], J.R. Pater[16], G.N. Patrick[20], J. Patt[10], R. Perez-Ochoa[8], P. Pfeifenschneider[14], J.E. Pilcher[9], J. Pinfold[28], D.E. Plane[8], B. Poli[2], J. Polok[8], M. Przybycień[8,d], A. Quadt[8], C. Rembser[8], H. Rick[8], S.A. Robins[21], N. Rodning[28], J.M. Roney[26], S. Rosati[3], K. Roscoe[16], A.M. Rossi[2], Y. Rozen[21], K. Runge[10], O. Runolfsson[8], D.R. Rust[12], K. Sachs[10], T. Saeki[23], O. Sahr[31], W.M. Sang[25], E.K.G. Sarkisyan[22], C. Sbarra[26], A.D. Schaile[31], O. Schaile[31], P. Scharff-Hansen[8], S. Schmitt[11], A. Schöning[8], M. Schröder[8], M. Schumacher[25], C. Schwick[8], W.G. Scott[20], R. Seuster[14,h], T.G. Shears[8], B.C. Shen[4], C.H. Shepherd-Themistocleous[5], P. Sherwood[15], G.P. Siroli[2], A. Skuja[17], A.M. Smith[8], G.A. Snow[17], R. Sobie[26], S. Söldner-Rembold[10,e], S. Spagnolo[20], M. Sproston[20], A. Stahl[3], K. Stephens[16], K. Stoll[10], D. Strom[19], R. Ströhmer[31], B. Surrow[8], S.D. Talbot[1], S. Tarem[21],

R.J. Taylor[15], R. Teuscher[9], M. Thiergen[10], J. Thomas[15], M.A. Thomson[8], E. Torrence[8], S. Towers[6], T. Trefzger[31], I. Trigger[8], Z. Trócsányi[30,g], E. Tsur[22], M.F. Turner-Watson[1], I. Ueda[23], R. Van Kooten[12], P. Vannerem[10], M. Verzocchi[8], H. Voss[3], D. Waller[6], C.P. Ward[5], D.R. Ward[5], P.M. Watkins[1], A.T. Watson[1], N.K. Watson[1], P.S. Wells[8], T. Wengler[8], N. Wermes[3], D. Wetterling[11] J.S. White[6], G.W. Wilson[16], J.A. Wilson[1], T.R. Wyatt[16], S. Yamashita[23], V. Zacek[18], D. Zer-Zion[8]

[1]School of Physics and Astronomy, University of Birmingham, Birmingham B15 2TT, UK

[2]Dipartimento di Fisica dell' Università di Bologna and INFN, I-40126 Bologna, Italy

[3]Physikalisches Institut, Universität Bonn, D-53115 Bonn, Germany

[4]Department of Physics, University of California, Riverside CA 92521, USA

[5]Cavendish Laboratory, Cambridge CB3 0HE, UK

[6]Ottawa-Carleton Institute for Physics, Department of Physics, Carleton University, Ottawa, Ontario K1S 5B6, Canada

[7]Centre for Research in Particle Physics, Carleton University, Ottawa, Ontario K1S 5B6, Canada

[8]CERN, European Organisation for Particle Physics, CH-1211 Geneva 23, Switzerland

[9]Enrico Fermi Institute and Department of Physics, University of Chicago, Chicago IL 60637, USA

[10]Fakultät für Physik, Albert Ludwigs Universität, D-79104 Freiburg, Germany

[11]Physikalisches Institut, Universität Heidelberg, D-69120 Heidelberg, Germany

[12]Indiana University, Department of Physics, Swain Hall West 117, Bloomington IN 47405, USA

[13]Queen Mary and Westfield College, University of London, London E1 4NS, UK

[14]Technische Hochschule Aachen, III Physikalisches Institut, Sommerfeldstrasse 26-28, D-52056 Aachen, Germany

[15]University College London, London WC1E 6BT, UK

[16]Department of Physics, Schuster Laboratory, The University, Manchester M13 9PL, UK

[17]Department of Physics, University of Maryland, College Park, MD 20742, USA

[18]Laboratoire de Physique Nucléaire, Université de Montréal, Montréal, Quebec H3C 3J7, Canada

[19]University of Oregon, Department of Physics, Eugene OR 97403, USA

[20]CLRC Rutherford Appleton Laboratory, Chilton, Didcot, Oxfordshire OX11 0QX, UK

[21]Department of Physics, Technion-Israel Institute of Technology, Haifa 32000, Israel

[22]Department of Physics and Astronomy, Tel Aviv University, Tel Aviv 69978, Israel

[23]International Centre for Elementary Particle Physics and Department of Physics, University of Tokyo, Tokyo 113-0033, and Kobe University, Kobe 657-8501, Japan

[24]Particle Physics Department, Weizmann Institute of Science, Rehovot 76100, Israel

[25]Universität Hamburg/DESY, II Institut für Experimental Physik, Notkestrasse 85, D-22607 Hamburg, Germany

[26]University of Victoria, Department of Physics, P O Box 3055, Victoria BC V8W 3P6, Canada

[27]University of British Columbia, Department of Physics, Vancouver BC V6T 1Z1, Canada

[28]University of Alberta, Department of Physics, Edmonton AB T6G 2J1, Canada

[29]Research Institute for Particle and Nuclear Physics, H-1525 Budapest, P O Box 49, Hungary

[30]Institute of Nuclear Research, H-4001 Debrecen, P O Box 51, Hungary

[31]Ludwigs-Maximilians-Universität München, Sektion Physik, Am Coulombwall 1, D-85748

Garching, Germany

[a] and at TRIUMF, Vancouver, Canada V6T 2A3
[b] and Royal Society University Research Fellow
[c] and Institute of Nuclear Research, Debrecen, Hungary
[d] and University of Mining and Metallurgy, Cracow
[e] and Heisenberg Fellow
[f] now at Yale University, Dept of Physics, New Haven, USA
[g] and Department of Experimental Physics, Lajos Kossuth University, Debrecen, Hungary
[h] and MPI München
[i] now at MPI für Physik, 80805 München.

1 Introduction

Bose-Einstein correlations (BECs) [1] in pairs of identical bosons, mainly $\pi^\pm\pi^\pm$, have been widely studied at various energies for hadronic final states produced by different initial states: e^+e^- [2, 3], ep [4], $p\bar{p}$ [5], πp, $K^\pm p$ [6] and heavy ion collisions [7]. Two-particle BECs have also been studied for $K^0_S K^0_S$ pairs [8], for $K^\pm K^\pm$ [9] and, at LEP2, for pions coming from W^+W^- decays [10]. Genuine BECs have also been observed for three charged identical pions [11].

BECs are manifested as enhancements in the production of identical bosons which are close to one another in phase space. They can be analysed in terms of the correlation function

$$\mathrm{C}(p_1, p_2) \;=\; \frac{\rho(p_1, p_2)}{\rho_0(p_1, p_2)}, \tag{1}$$

where p_1 and p_2 are the four-momenta of the two bosons, $\rho(p_1, p_2)$ is the measured density of the two identical bosons and $\rho_0(p_1, p_2)$ is the two-particle density in the absence of BECs. The choice of the reference sample used to determine $\rho_0(p_1, p_2)$ is crucial for the measurement. It should have the same properties as the sample used for $\rho(p_1, p_2)$ except for the presence of BECs. In this paper we use pairs of particles with charges of opposite sign as the reference sample. This sample, however, includes pairs coming from resonance decays and from weakly decaying particles, like the K^0_S. In addition, the correlation function obtained with this reference sample has to be normalized and suffers, at large four-momentum differences, from long-range correlations due to energy, momentum and charge conservation. We therefore also use a large sample of Monte Carlo events without the simulation of Bose-Einstein effects in order to obtain a correlation function which is self normalized and which has a reduced contamination from correlated unlike-charge pairs. This correlation function, called $\mathrm{C}'(p_1, p_2)$, is used in the paper to obtain the reference results.

The information obtained from the shape of the correlation function may be used to infer the space-time extent of the particle emitting region. Most analyses have been performed assuming a spherical emitter but several theoretical investigations have recently treated the shape of the correlation function in more than one dimension [12]. The Lund group, in particular, has developed a model for BECs based on a quantum mechanical interpretation of the string area fragmentation probability [13]. One of the main predictions of the model, developed for two-jet events, is that, since momentum components longitudinal and transverse with respect to the string direction (i.e. event direction) are generated by different mechanisms, the correlation length in the longitudinal direction is different from that in the transverse one. In particular, in the so called Longitudinally CoMoving System (LCMS), the longitudinal source dimension is predicted to be larger than the transverse dimension.

In this paper we describe an experimental study of transverse and longitudinal BECs performed with the high statistics sample of hadronic events recorded by the OPAL detector at LEP at centre-of-mass energies at and near the Z^0 resonance. Similar two- and three-dimensional studies have been done in e^+e^- annihilations at centre-of-mass energies of 34 GeV [14] and 91 GeV [15]. We also present the results of a unidimensional analysis of BECs.

4

2 Detector and Data Selection

A detailed description of the OPAL detector can be found in refs. [16, 17]. This analysis is based mainly on the reconstruction of charged particle trajectories and momenta in the central tracking chambers and on energy deposits ("clusters") in the electromagnetic calorimeters. All tracking systems are located inside a solenoidal magnet which provides a uniform magnetic field of 0.435 T along the beam axis [1]. The magnet is surrounded by a lead-glass electromagnetic calorimeter and a hadron calorimeter of the sampling type. Outside the hadron calorimeter, the detector is surrounded by a system of muon chambers. There are similar layers of detectors in the barrel ($|\cos\theta| < 0.82$) and endcap ($|\cos\theta| > 0.81$) regions. The central tracking detector consists of a silicon micro-vertex detector [17], close to the beam pipe, and three drift chamber devices: the vertex detector, a large jet chamber, and surrounding z-chambers. The vertex chamber is a cylindrical drift chamber covering a range of $|\cos\theta| < 0.95$ with a resolution of $50\,\mu$m in the $r\phi$ plane and $700\,\mu$m in the z direction. The jet chamber is a cylindrical drift chamber with an inner radius of 25 cm, an outer radius of 185 cm, and a length of about 4 m. Its spatial resolution is about $135\,\mu$m in the $r\phi$ plane from drift time information and about 6 cm in the z direction from charge division. The z-chambers provide a more accurate z measurement, with a resolution of about $300\,\mu$m. In combination, the three drift chambers yield a momentum resolution of $\sigma_{p_t}/p_t \approx \sqrt{0.02^2 + (0.0015 \cdot p_t)^2}$ for $|\cos(\theta)| < 0.7$, where p_t is the transverse momentum in GeV/c. Electromagnetic energy is measured by lead-glass calorimeters surrounding the solenoid magnet coil. They consist of a barrel and two endcap arrays with a total of 11704 lead-glass blocks covering a range of $|\cos\theta| < 0.98$.

A number of selection cuts are applied to the initial data sample, consisting of $4.3 \cdot 10^6$ hadronic events from Z^0 decays. In order to be considered, a charged track is required to have a minimum of 20 hits in the jet chamber, a minimum transverse momentum of 150 MeV/c and a maximum momentum p of 65 GeV/c. Clusters in the electromagnetic calorimeter are used in the jet-finding algorithm if their energies exceed 100 MeV in the barrel, or 200 MeV in the endcaps. Only events that are well contained in the detector are accepted, by requiring that $|cos\theta_{thrust}| < 0.9$, where θ_{thrust} is the polar angle of the thrust axis, computed using charged tracks and electromagnetic clusters that passed the above cuts. A second set of cuts, specific to the BEC analysis, is then applied. Tracks are required to have a total momentum $p < 40$ GeV/c and to come from the interaction vertex. Electron-positron pairs from photon conversions are rejected. Events are selected if they contain a minimum number of five charged tracks and if reasonably balanced in charge, i.e. if $|n_{ch}^+ - n_{ch}^-|/(n_{ch}^+ + n_{ch}^-) \leq 0.4$, where n_{ch}^+ and n_{ch}^- are the number of positive and negative charged tracks, respectively. The analysis is performed on the inclusive sample of all events passing the above cuts. In order to compare the experimental results with the predictions of [13], which are relevant to two-jet events, and to study the dependence of the results on the "jettyness" of the event the same analysis is done on samples of events defined as "two-jet events" by the Durham jet-finding algorithm [18], with various values of the resolution parameter y_{cut}.

---

[1] The coordinate system is defined so that z is the coordinate parallel to the e$^+$ and e$^-$ beams, with positive direction along the e$^-$ beam; r is the coordinate normal to the beam axis, ϕ is the azimuthal angle and θ is the polar angle with respect to $+z$.
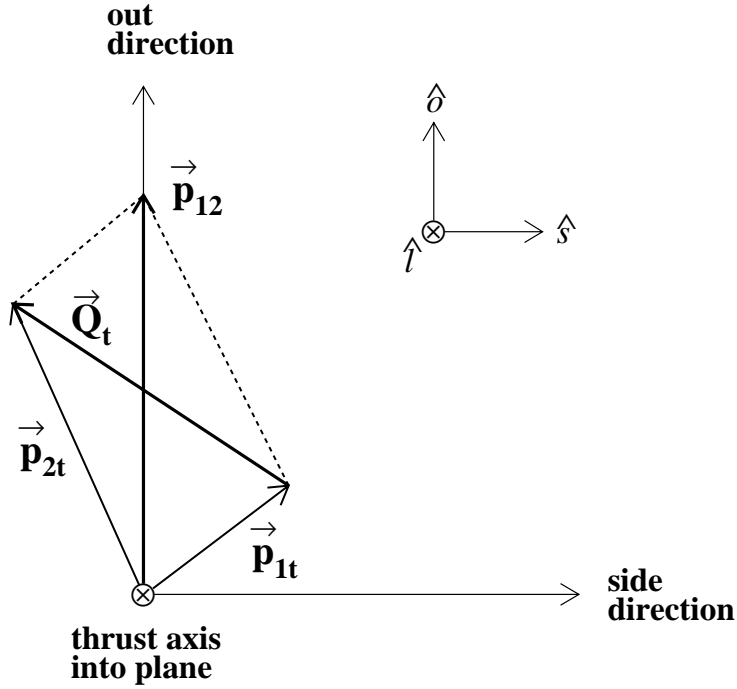
Figure 1: *The LCMS frame of reference drawn for a pair of particles where $\vec{p}_{1t}$ and $\vec{p}_{2t}$ are the projections of the two particles momenta onto the plane perpendicular to the thrust axis.*

3   The Longitudinally CoMoving System

In order to study transverse and longitudinal BECs, we define variables in the LCMS [19]. Given a pair of particles, the LCMS is the frame of reference in which the sum of the two particle momenta, $\vec{p}_{12} = (\vec{p}_1 + \vec{p}_2)$, lies in the plane perpendicular to the thrust axis (see Fig. 1, where $\vec{p}_{1t}$ and $\vec{p}_{2t}$ are the projections onto the plane). The momentum difference of the pair, $\vec{Q} = (\vec{p}_2 - \vec{p}_1)$, computed in the LCMS, is resolved into the moduli of the transverse component, $\vec{Q}_t$, defined as shown in Fig. 1, and of the longitudinal component

$$\vec{Q}_l = |p'_{l_2} - p'_{l_1}|\hat{l} \tag{2}$$

where the $\hat{l}$ direction coincides with the thrust axis. The momentum components are marked with a prime when they are measured in the LCMS. $\vec{Q}_t$ may in turn be resolved into "out", $Q_{t_{out}}$, and "side", $Q_{t_{side}}$, components

$$\vec{Q}_t = Q_{t_{out}}\hat{o} + Q_{t_{side}}\hat{s} \tag{3}$$

where $\hat{o}$ and $\hat{s}$ are unit vectors in the plane perpendicular to the thrust direction, such that $\vec{p}_{12} = p_{12}\hat{o}$ defines the "out" direction and $\hat{s} = \hat{l} \times \hat{o}$ defines the "side" direction. The symbol Q is used for the invariant modulus of the four-momentum difference $Q = [|E_2 - E_1|, (\vec{p}_2 - \vec{p}_1)]$.

It can be shown (see for instance ref. [20]) that, in the LCMS, the components $Q_{t_{side}}$ and Q_l reflect only the difference in emission space of the two pions, while $Q_{t_{out}}$ depends on the difference in emission time as well. Indeed, the scalar product between Q and the four-vector $P = [(E_2 + E_1), (\vec{p}_2 + \vec{p}_1)]$ is, in the LCMS

$$Q \cdot P = (E'_2 - E'_1)(E'_2 + E'_1) - Q_{t_{out}}p_{12}. \tag{4}$$

6

Since $Q \cdot P = 0$, then

$$Q^2 = (E_2' - E_1')^2 - Q_{t_{out}}^2 - Q_{t_{side}}^2 - Q_l^2 = ((\frac{p_{12}}{E_2' + E_1'})^2 - 1)Q_{t_{out}}^2 - Q_{t_{side}}^2 - Q_l^2. \quad (5)$$

Therefore, the BECs evaluated with respect to $Q_{t_{side}}$ and Q_l in the LCMS yield information on the geometrical dimensions of the pion emitting source. In the string model [13] LCMS represents the local rest frame of the string. In the following, we shall study the Bose-Einstein correlation function using two different definitions of the reference sample.

4 The Bose-Einstein Correlation function

The three-dimensional correlation function C is defined, in a small phase space volume around each triplet of $Q_{t_{out}}$, $Q_{t_{side}}$ and Q_l values, as the number of like-charge pairs in that volume divided by the number of unlike-charge pairs, used as a reference sample:

$$C(Q_{t_{out}}, Q_{t_{side}}, Q_l) = \frac{N_{\pi^+\pi^+} + N_{\pi^-\pi^-}}{N_{\pi^+\pi^-}} = \frac{N_{like}}{N_{unlike}}. \quad (6)$$

Coulomb interactions between charged particles affect differently like- and unlike-charge pairs and thus modify the correlation function. A correction, based on the Gamow factors [21], is applied: each pair of like-charge pions is weighted by a factor

$$G_l(Q) = (e^{2\pi\eta} - 1)/2\pi\eta , \quad (7)$$

where $\eta = \alpha_{em} m_\pi/Q$; each pair of unlike-charge pions is weighted by a factor

$$G_u(Q) = (1 - e^{-2\pi\eta})/2\pi\eta . \quad (8)$$

The use of unlike-charge pairs as a reference sample gives large distortions of the correlation function in some regions of the domain $(Q_{t_{out}}, Q_{t_{side}}, Q_l)$, caused by the presence of correlated $\pi^+\pi^-$ pairs originating from decays of hadron resonances and of weakly decaying particles. In order to correct the correlation function, the $Q_{t_{out}}$, $Q_{t_{side}}$ and Q_l distribution of the decay products of ω, η, η', K_S^0, ρ^0, $f_0(980)$ and $f_2(1270)$ is determined for a sample of Jetset 7.4 [22] multihadronic Monte Carlo events. Their contribution, due mainly to ω, η, K_S^0 and ρ^0, is subtracted from the unlike pion distribution N_{unlike}. The OPAL version of Jetset used here reproduces the resonance structures reasonably well, although not perfectly. In particular the shape of the ρ^0 ($0.64 \leq Q \leq 0.80$ GeV) is not well modelled. For each resonance, differences between the simulated and measured [23] resonance rates are taken into account by scaling the distribution using the ratio of the measured production rate and the corresponding rate in Jetset. The resonance distributions obtained are then summed and scaled by the number of selected events. Figure 2 shows the distribution N_{unlike} in the one-dimensional variable Q. The contribution of the decay products and the same distribution after the subtraction of this contribution are also shown. Two-dimensional projections of the function $C(Q_{t_{out}}, Q_{t_{side}}, Q_l)$, after the correction for Coulomb and resonance decay effects, are shown in Fig. 3 for the sample of two-jet events selected, as an example, with $y_{cut} = 0.04$ and with the third component, not plotted, limited to values up to 200 MeV. The histogram bin size, 40 MeV, is chosen to match the momentum resolution of the detector. The presence of Bose-Einstein correlations is seen as the sharp peak at small values of $Q_{t_{out}}$, $Q_{t_{side}}$ and Q_l.
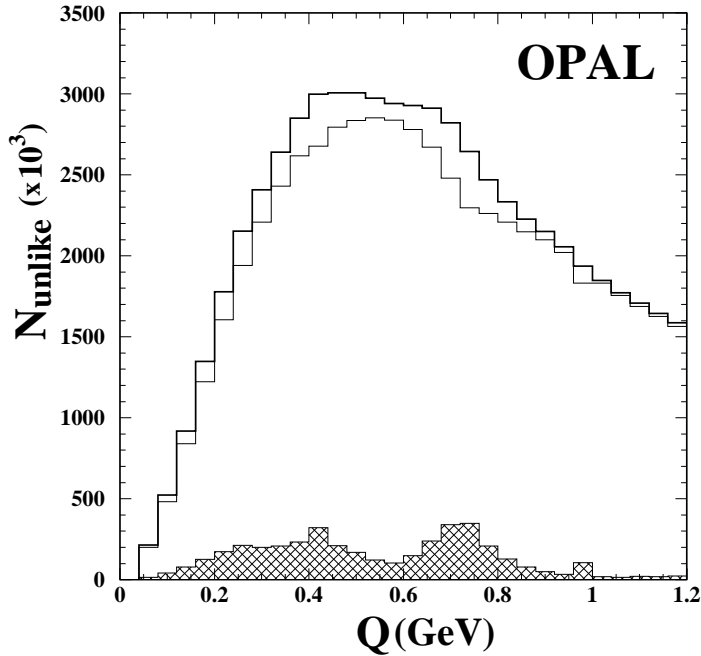
Figure 2: *The unlike-charge pairs distribution vs Q before (thick line) and after (thin line) the subtraction of the contribution from resonance decays (filled histograms; the higher peak is due to the ρ^0, the lower structure to the ω^0, η and K_S^0).*

5 Parametrisation of the Correlation function

A minimum χ^2 fit to the measured three-dimensional correlation function is performed using the following extended Goldhaber [24] parametrisation:

$$\mathrm{C}(\mathrm{Q}_{t_{out}}, \mathrm{Q}_{t_{side}}, \mathrm{Q}_l) = \mathrm{N}(1 + \lambda e^{-(\mathrm{Q}_{t_{out}}^2 r_{t_{out}}^2 \; + \; \mathrm{Q}_{t_{side}}^2 r_{t_{side}}^2 \; + \; \mathrm{Q}_l^2 r_l^2)})\mathrm{F}(\mathrm{Q}_{t_{out}}, \mathrm{Q}_{t_{side}}, \mathrm{Q}_l) \qquad (9)$$

with

$$\mathrm{F}(\mathrm{Q}_{t_{out}}, \mathrm{Q}_{t_{side}}, \mathrm{Q}_l) = (1 + \delta_{t_{out}}\mathrm{Q}_{t_{out}} + \delta_{t_{side}}\mathrm{Q}_{t_{side}} + \delta_l\mathrm{Q}_l + \epsilon_{t_{out}}\mathrm{Q}_{t_{out}}^2 + \epsilon_{t_{side}}\mathrm{Q}_{t_{side}}^2 + \epsilon_l\mathrm{Q}_l^2). \quad (10)$$

The chaoticity parameter λ measures the strength of the correlation, $r_{t_{out}}$, $r_{t_{side}}$ and r_l indicate the transverse and longitudinal extent of the two-pion source, N is a normalization factor necessary since the reference sample N_{unlike} is not normalized to the sample of like-charge pairs. The term $\mathrm{F}(\mathrm{Q}_{t_{out}}, \mathrm{Q}_{t_{side}}, \mathrm{Q}_l)$ accounts for long-range two-particle correlations, due to energy and charge conservation and to phase space constraints. Alternative forms for this function have been considered, as in particular a fit with only the linear long-range terms $\delta_i\mathrm{Q}_i$ ($i = t_{out}$, t_{side}, l), and the results did not change significantly. The best results (lower values of χ^2/DoF and stability) are obtained with formula (10). The fits are performed over the range $0.04 \le \mathrm{Q}_{t_{out}}, \mathrm{Q}_{t_{side}}, \mathrm{Q}_l \le 1.2$ GeV. The region below 0.04 GeV is excluded because of the limited momentum resolution at low Q_i values and of the presence of residual photon conversion pairs. Even after the subtraction procedure described in section 4, a few regions show significant distortions (see Fig. 3) assumed to be due to residual effects of pairs coming from resonance decays: these regions, corresponding to $0.28 \le \sqrt{\mathrm{Q}_{t_{out}}^2 + \mathrm{Q}_{t_{side}}^2 + \mathrm{Q}_l^2} \le 0.44$ GeV and $0.64 \le \sqrt{\mathrm{Q}_{t_{out}}^2 + \mathrm{Q}_{t_{side}}^2 + \mathrm{Q}_l^2} \le 0.80$ GeV, are not used in the fits.

8

OPAL

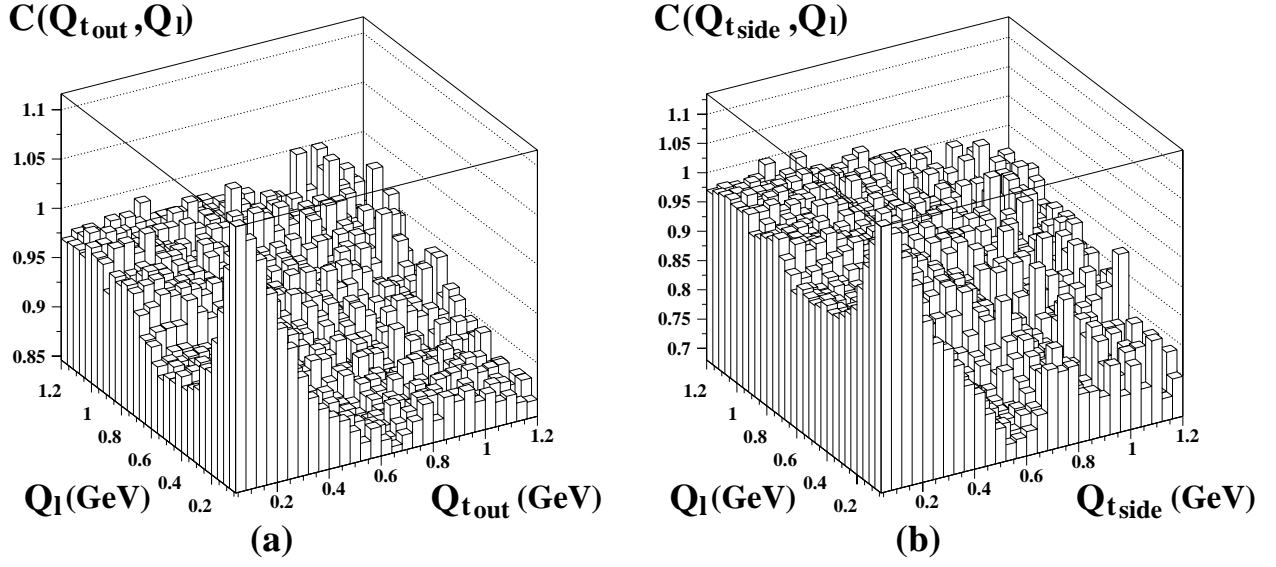C($Q_{t_{out}}$,Q_l)

C($Q_{t_{side}}$,Q_l)

(a)

(b)

Figure 3: *The projections of the three-dimensional correlation function C($Q_{t_{out}}$,$Q_{t_{side}}$,Q_l), for two-jet events selected with $y_{cut} = 0.04$, onto the (a) $Q_{t_{out}}$-Q_l and the (b) $Q_{t_{side}}$-Q_l planes when the third component has values up to 200 MeV. Notice the different behaviour of C as function of $Q_{t_{side}}$ and Q_l.*

Parameter	$y_{cut} = 0.01$	$y_{cut} = 0.02$	$y_{cut} = 0.04$	$y_{cut} = 0.06$	inclusive sample
N	0.803 ± 0.002	0.815 ± 0.001	0.825 ± 0.001	0.831 ± 0.001	0.842 ± 0.001
λ	0.479 ± 0.005	0.464 ± 0.004	0.454 ± 0.004	0.446 ± 0.004	0.442 ± 0.004
$r_{t_{out}}$ [fm]	0.522 ± 0.007	0.520 ± 0.007	0.525 ± 0.006	0.523 ± 0.006	0.536 ± 0.006
$r_{t_{side}}$ [fm]	0.750 ± 0.007	0.767 ± 0.006	0.783 ± 0.006	0.787 ± 0.006	0.809 ± 0.006
r_l [fm]	1.013 ± 0.011	1.014 ± 0.010	1.015 ± 0.009	1.011 ± 0.009	1.018 ± 0.009
$\delta_{t_{out}}$ [GeV^{-1}]	-0.015 ± 0.004	-0.010 ± 0.004	-0.003 ± 0.003	-0.002 ± 0.003	0.004 ± 0.003
$\delta_{t_{side}}$ [GeV^{-1}]	-0.149 ± 0.004	-0.148 ± 0.004	-0.146 ± 0.003	-0.145 ± 0.003	-0.142 ± 0.003
δ_l [GeV^{-1}]	0.300 ± 0.005	0.262 ± 0.004	0.228 ± 0.004	0.212 ± 0.004	0.178 ± 0.003
$\epsilon_{t_{out}}$ [GeV^{-2}]	0.001 ± 0.004	0.010 ± 0.003	0.013 ± 0.003	0.015 ± 0.003	0.015 ± 0.002
$\epsilon_{t_{side}}$ [GeV^{-2}]	-0.032 ± 0.004	0.000 ± 0.004	0.022 ± 0.003	0.034 ± 0.003	0.053 ± 0.003
ϵ_l [GeV^{-2}]	-0.072 ± 0.004	-0.055 ± 0.003	-0.039 ± 0.003	-0.031 ± 0.003	-0.016 ± 0.002
χ^2/DoF	30089/24428	31529/24428	32758/24428	33261/24428	34632/24428
$r_l/r_{t_{side}}$	1.351 ± 0.027	1.322 ± 0.025	1.296 ± 0.021	1.285 ± 0.021	1.258 ± 0.020

Table 1: *Results of the fits of Eq. 9 to the measured three-dimensional correlation function C($Q_{t_{out}}$,$Q_{t_{side}}$,Q_l) over the range $0.04 \leq Q_{t_{out}},Q_{t_{side}},Q_l \leq 1.2$ GeV, excluding the regions affected by residual resonance decay products described in the text. The quoted errors are statistical uncertainties obtained from the fits. The quality of the fits is indicated by the value of χ^2/DoF.*

The values of the parameters resulting from the fits to the correlation functions for two-jet events (with different values of y_{cut}) and for the inclusive sample are given in Table 1. For all the fits, the transverse and longitudinal radii are significantly different. In particular, the ratio $r_l/r_{t_{side}}$ between the longitudinal and transverse source radii is $r_l/r_{t_{side}} = 1.296 \pm 0.021$ (*stat*) for two-jet events selected with $y_{cut} = 0.04$ and $r_l/r_{t_{side}} = 1.258 \pm 0.020$ (*stat*) for the inclusive
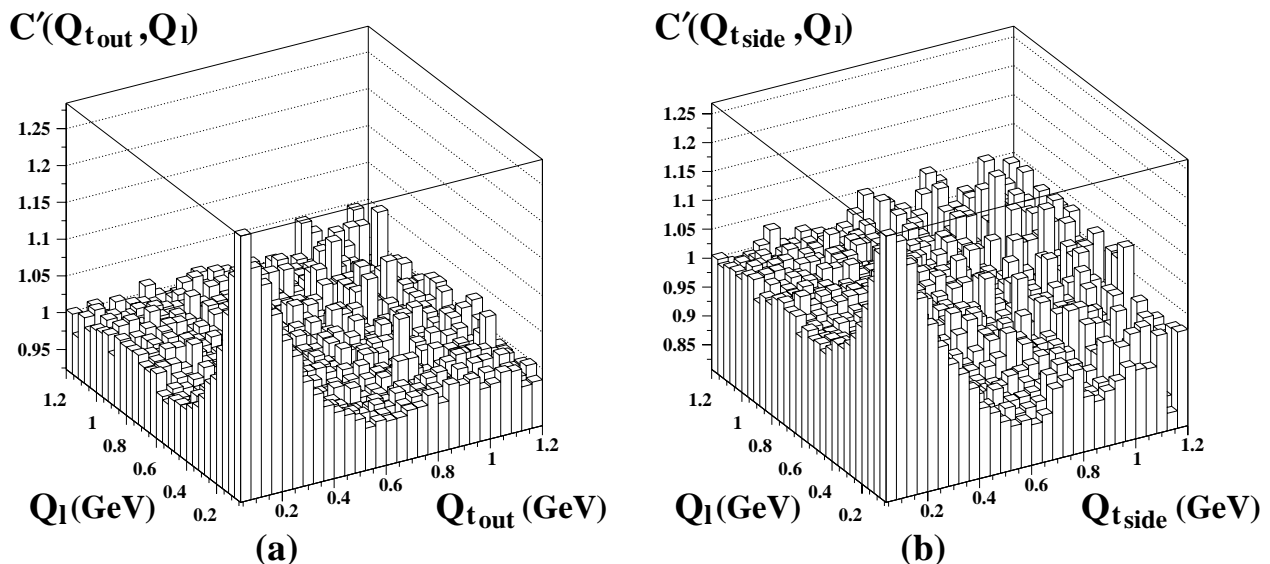
9

C′(Q$_{t_{out}}$,Q$_l$)

C′(Q$_{t_{side}}$,Q$_l$)

(a)

(b)

Figure 4: *The projections of the three-dimensional correlation function C′($Q_{t_{out}}$,$Q_{t_{side}}$,Q_l), for two-jet events selected with y_{cut} = 0.04, onto the (a) $Q_{t_{out}}$-Q_l and the (b) $Q_{t_{side}}$-Q_l planes when the third component has values up to 200 MeV. Notice the different behaviour of C′ as function of $Q_{t_{side}}$ and Q_l.*

sample of events.

6   The Correlation function $C' = C^{DATA}/C^{MC}$

In order to improve the quality of the Goldhaber fits, reducing the effects from long-range correlations and resonance decay products, it is usual to define the following ratio of correlation functions, using data and Monte Carlo events:

$$C'(Q_{t_{out}}, Q_{t_{side}}, Q_l) \;=\; \frac{C^{DATA}}{C^{MC}} \;=\; \frac{N_{like}^{DATA}/N_{unlike}^{DATA}}{N_{like}^{MC}/N_{unlike}^{MC}}. \tag{11}$$

For this purpose, a sample of 7.2 million Jetset 7.4 multihadronic Monte Carlo events, which does not include BEC effects, is used. The Monte Carlo simulates many of the dynamical correlations present in the real data but not the Coulomb effect. Therefore, in Eq. 11, only N_{like}^{DATA} and N_{unlike}^{DATA} are corrected by the Gamow factors given in (7) and (8). The simulation includes the resonance decay products. The correction, due to the differences in the measured and simulated resonance rates, is done by subtracting (adding) to the unlike-charge pairs sample in the Monte Carlo the fraction of pairs simulated in excess (deficit). Two- and one-dimensional projections of the correlation function C′, for the sample of two-jet events selected with $y_{cut} = 0.04$, are shown in Fig. 4 and in Fig. 5, respectively. The Bose-Einstein correlations are clearly visible at small $Q_{t_{out}}$, $Q_{t_{side}}$ and Q_l. The fits of Eq. 9, yield the parameters given in Table 2. As can be seen in the Table, the correlation function C′ is almost normalized; the slight difference from 1.0 is due to the difference in the average multiplicity between data and MonteCarlo. The χ^2/DoF values for these fits are closer to unity than for those relative to the correlation function C. The dependences of $r_{t_{out}}$, $r_{t_{side}}$, r_l and of the ratios $r_l/r_{t_{out}}$, $r_l/r_{t_{side}}$ on the jet resolution parameter
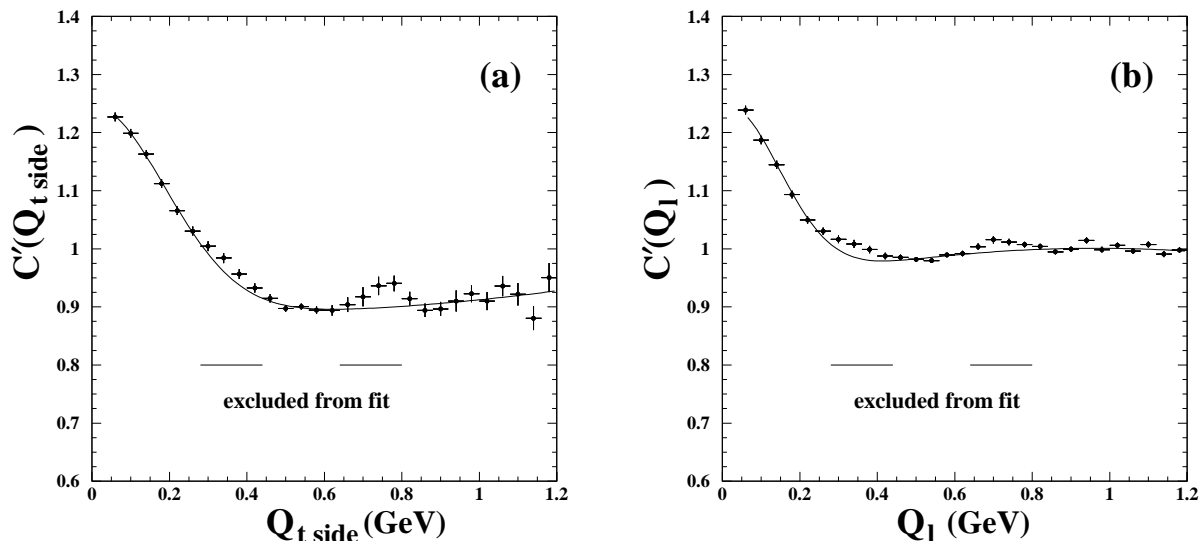
10

Figure 5: *The projections of the three-dimensional correlation function $C'(Q_{t_{out}}, Q_{t_{side}}, Q_l)$, for two-jet events selected with $y_{cut} = 0.04$, onto the (a) $Q_{t_{side}}$ and (b) Q_l axes when the two other components have values up to 200 MeV.*

Parameter	$y_{cut} = 0.01$	$y_{cut} = 0.02$	$y_{cut} = 0.04$	$y_{cut} = 0.06$	inclusive sample
N	0.947 ± 0.002	0.950 ± 0.002	0.952 ± 0.002	0.954 ± 0.001	0.957 ± 0.001
λ	0.457 ± 0.006	0.446 ± 0.005	0.443 ± 0.005	0.441 ± 0.005	0.437 ± 0.004
$r_{t_{out}}$ [fm]	0.678 ± 0.013	0.654 ± 0.012	0.647 ± 0.011	0.637 ± 0.010	0.621 ± 0.010
$r_{t_{side}}$ [fm]	0.781 ± 0.010	0.794 ± 0.009	0.809 ± 0.009	0.814 ± 0.008	0.831 ± 0.008
r_l [fm]	0.987 ± 0.013	0.989 ± 0.012	0.989 ± 0.011	0.989 ± 0.010	0.992 ± 0.010
$\delta_{t_{out}}$ [GeV^{-1}]	-0.004 ± 0.005	-0.002 ± 0.004	0.006 ± 0.004	0.005 ± 0.004	0.008 ± 0.003
$\delta_{t_{side}}$ [GeV^{-1}]	-0.062 ± 0.005	-0.071 ± 0.004	-0.075 ± 0.004	-0.077 ± 0.004	-0.079 ± 0.003
δ_l [GeV^{-1}]	0.114 ± 0.005	0.103 ± 0.005	0.092 ± 0.004	0.086 ± 0.004	0.073 ± 0.003
$\epsilon_{t_{out}}$ [GeV^{-2}]	0.012 ± 0.004	0.016 ± 0.004	0.012 ± 0.003	0.013 ± 0.003	0.011 ± 0.003
$\epsilon_{t_{side}}$ [GeV^{-2}]	-0.020 ± 0.005	0.004 ± 0.004	0.019 ± 0.004	0.027 ± 0.004	0.037 ± 0.003
ϵ_l [GeV^{-2}]	-0.045 ± 0.004	-0.039 ± 0.004	-0.032 ± 0.003	-0.028 ± 0.003	-0.021 ± 0.003
χ^2/DoF	24654/24428	25249/24428	25398/24428	25482/24428	25836/24428
$r_l/r_{t_{side}}$	1.264 ± 0.033	1.246 ± 0.029	1.222 ± 0.027	1.215 ± 0.024	1.194 ± 0.024

Table 2: *Results of the fits of Eq. 9 to the measured three-dimensional correlation function $C'(Q_{t_{out}}, Q_{t_{side}}, Q_l)$ over the range $0.04 \leq Q_{t_{out}}, Q_{t_{side}}, Q_l \leq 1.2$ GeV, excluding the regions affected by residual resonance decay products described in the text. The quoted errors are the statistical uncertainties obtained from the fits. The quality of the fits is indicated by the value of χ^2/DoF.*

y_{cut} are shown in Fig. 6, where the results for inclusive events are also presented. The main features of the results are a very slight decrease and increase, respectively, of $r_{t_{out}}$ and $r_{t_{side}}$ as y_{cut} increases, while r_l is independent of the y_{cut}. The ratio $r_l/r_{t_{out}}$ increases slightly, while $r_l/r_{t_{side}}$ decreases when y_{cut} increases. The value of the chaoticity parameter λ is between 0.457 and 0.437 (decreasing slowly with y_{cut}).
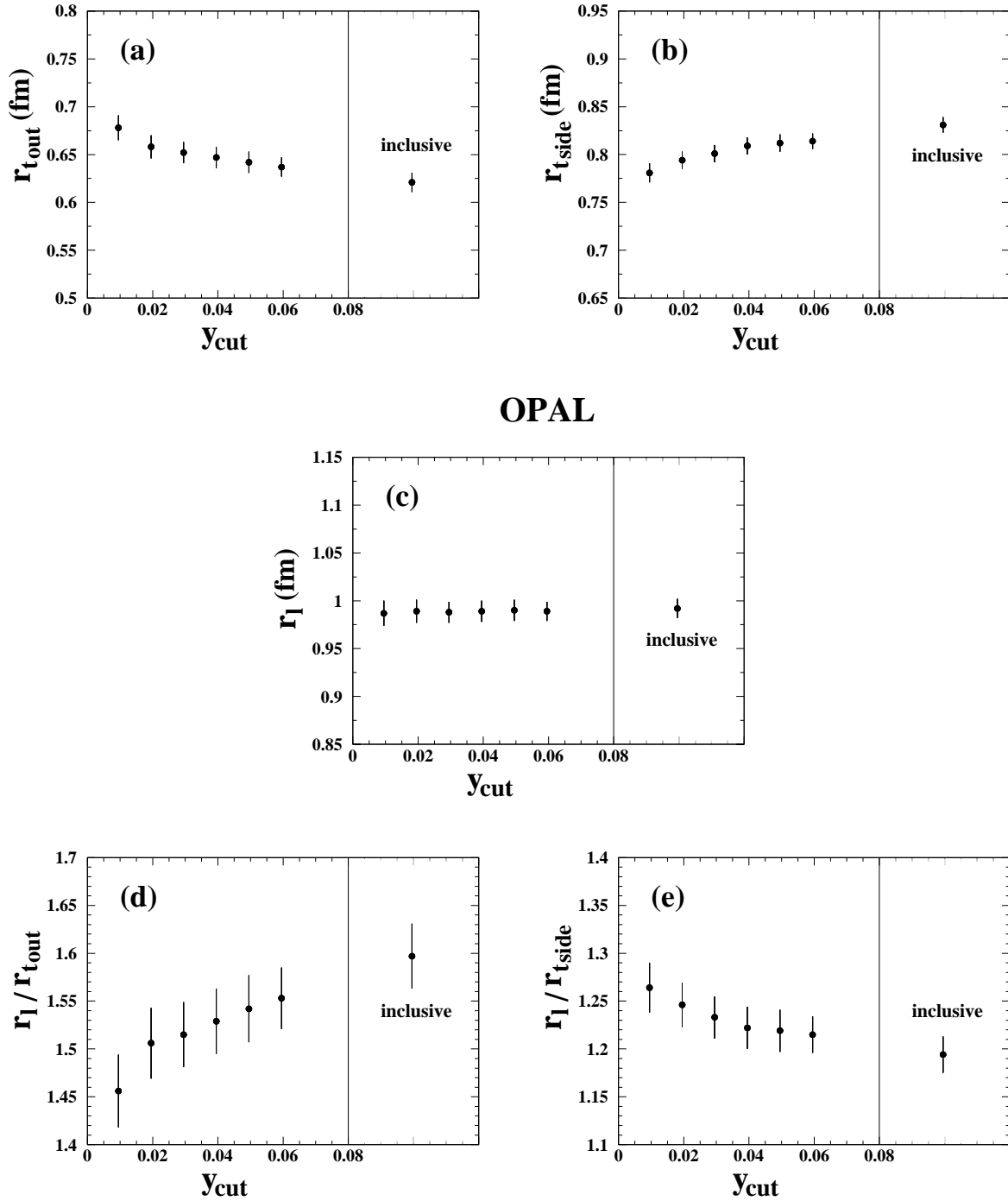
OPAL

Figure 6: *Dependence on the resolution parameter y_{cut} of (a) $r_{t_{out}}$, (b) $r_{t_{side}}$ and (c) r_l and of the ratios (d) $r_l/r_{t_{out}}$ and (e) $r_l/r_{t_{side}}$ for the correlation function $C'(Q_{t_{out}}, Q_{t_{side}}, Q_l)$.*

The systematic uncertainties on the parameter values are estimated considering the deviations with respect to a reference analysis, chosen to be the fit of Eq. 9 performed to the correlation function $C'(Q_{t_{out}}, Q_{t_{side}}, Q_l)$ for two-jet events selected with $y_{cut} = 0.04$. In this case we have $r_l/r_{t_{side}} = 1.222 \pm 0.027$ (*stat*). The analysis is repeated changing some of the selection cuts: a maximum total momentum $p < 30$ GeV/c instead of $p < 40$ GeV/c and a charge unbalance smaller than 0.25 per event instead of 0.4. In order to check the stability of the results on the method used to correct the unlike-charge distribution for K_S^0 and resonance de-

12

cay products, the measured resonance rates are varied inside the experimental errors to obtain maximum and minimum values for the factors used to correct (i.e. either subtracted or added according to a defect or an excess with respect to the simulated resonance rates) N_{unlike}^{MC}. To estimate the influence of the long-range correlations, the fit is performed in a more restricted interval, $0.04 \leq Q_{t_{out}}$, $Q_{t_{side}}$,$Q_l \leq 1.0$ GeV. Finally, the difference between the results of the fits to the correlation functions C and C′ is considered as an asymmetrical contribution to the systematic error. Table 3 shows the various contributions to the systematic error. The global

	$r_{t_{out}}$ [fm]	$r_{t_{side}}$ [fm]	r_l [fm]	$r_l/r_{t_{side}}$	χ^2/DoF
a) Reference fit	0.647 ± 0.011	0.809 ± 0.009	0.989 ± 0.011	1.222 ± 0.027	25398/24428
b) Modified track selection	0.656 ± 0.012	0.815 ± 0.009	0.995 ± 0.012	1.221 ± 0.028	25209/24428
c) Max. resonance correction	0.639 ± 0.010	0.812 ± 0.008	0.988 ± 0.010	1.217 ± 0.024	25566/24428
c) Min. resonance correction	0.657 ± 0.011	0.805 ± 0.009	0.989 ± 0.011	1.228 ± 0.027	25319/24428
d) Restricted fit range	0.627 ± 0.012	0.791 ± 0.009	0.975 ± 0.011	1.233 ± 0.028	13751/13053
e) Correlation function C	0.525 ± 0.006	0.783 ± 0.006	1.015 ± 0.009	1.296 ± 0.021	32758/24428

Table 3: *Results of the fit of Eq. 9 to several variations of C′(Q$_{t_{out}}$,Q$_{t_{side}}$, Q$_l$), as listed in the text and in the first column. The quoted errors are only statistical.*

systematic uncertainties are computed by adding in quadrature the differences between the reference fit a) and the variations b) – e).

The conclusion from this analysis is that, as observed in the LCMS, the pion emitting region is elongated, with r_l greater than $r_{t_{side}}$. From Fig. 6 it is evident that the ratio $r_l/r_{t_{side}}$ has a (small) dependence on y_{cut}; the largest value is obtained for smaller y_{cut}. One also observes that r_l is independent on y_{cut}, while $r_{t_{side}}$ increases with increasing y_{cut}. As an example, we quote the following parameter values obtained for two-jet events, selected using $y_{cut} = 0.04$:

$$r_{t_{out}} = (0.647 \pm 0.011 \ (stat) \ ^{+0.024}_{-0.124} \ (syst)) \ \text{fm}$$

$$r_{t_{side}} = (0.809 \pm 0.009 \ (stat) \ ^{+0.019}_{-0.032} \ (syst)) \ \text{fm}$$

$$r_l = (0.989 \pm 0.011 \ (stat) \ ^{+0.030}_{-0.015} \ (syst)) \ \text{fm}$$

$$\text{(12)}$$

$$r_l/r_{t_{side}} = 1.222 \pm 0.027 \ (stat) \ ^{+0.075}_{-0.012} \ (syst).$$

The results of this analysis are in qualitative agreement with recent results from the L3 collaboration [15]. In the L3 analysis, which uses an event-mixing technique to compute the reference sample, the ratio of transverse to longitudinal radius is $0.81 \pm 0.02 \ ^{+0.03}_{-0.19}$, corresponding to $r_l/r_{t_{side}} = 1.23 \pm 0.03 \ ^{+0.29}_{-0.05}$.

The results can also be compared with the predictions of a recent model of BECs based on string fragmentation [13]. In this model, the different mechanisms that generate the longitudinal (i.e. along the string) and transverse momenta of the particle, lead to a longitudinal correlation length, representing the space-time difference along the string between the production points, which is larger than the transverse correlation length.
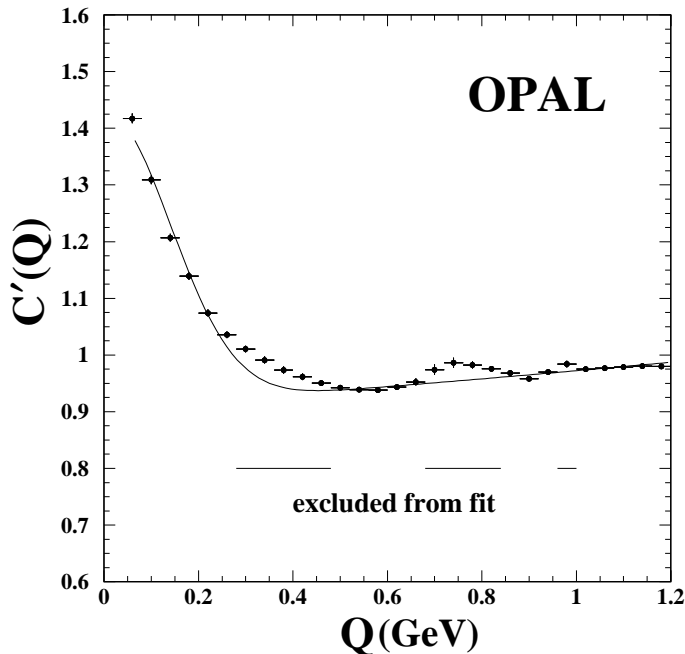
Figure 7: *The one-dimensional correlation function C'(Q) with the result of the one-dimensional Goldhaber fit, Eq. 13, superimposed.*

As a check, a two-dimensional analysis where the transverse component Q_t of the pair momentum difference is not split into "out" and "side" components, is done. The two-dimensional Goldhaber function fitted to the correlation function $C'(Q_t,Q_l)$ gives, in the case of two-jet events selected with $y_{cut} = 0.04$, $r_l/r_t = 1.360 \pm 0.026$ (*stat*), in agreement with a longitudinal source size larger than the transverse size. While $r_{t_{out}}$ and $r_{t_{side}}$ show a slight dependence on the jet resolution parameter y_{cut} (in opposite directions, see Fig. 6), the parameter r_t obtained from the two-dimensional analysis is independent on y_{cut}.

We conclude that we always have $r_l/r_{t_{side}}$ greater than one.

7 One-dimensional analysis of the inclusive sample

The one-dimensional correlation functions C(Q) and C'(Q), where Q is the modulus of the four-momentum difference of the pion pair, are studied for the inclusive sample. The results can be compared with those published in [2]; the present analysis uses more data (4.3 million Z^0 hadronic decays instead of 3.6 millions) and a different version of the Jetset Monte Carlo (7.4 instead of 7.3). The correlation function C'(Q), after the corrections for Coulomb and resonance decay products, is shown in Fig. 7. The one-dimensional Goldhaber function

$$C'(Q) = N(1 + \lambda e^{-Q^2 r^2})(1 + \delta Q + \epsilon Q^2) \tag{13}$$

is fitted to the measured correlation function over the range $0.04 \leq Q \leq 1.2$ GeV. There are apparent distortions in the unlike-charge pairs distribution even after the correction for the contribution of resonance decays products, as discussed in the three-dimensional analysis. Therefore the Q regions affected most by ω, η, K_S^0, ρ^0 and $f_0(980)$ decay products, corresponding respectively to $0.28 \leq Q \leq 0.48$ GeV, $0.68 \leq Q \leq 0.84$ GeV and $0.96 \leq Q \leq 1.0$ GeV, are excluded from the fit range.

14

	r [fm]	λ	χ^2/DoF
a) Reference fit	1.002 ± 0.016	0.574 ± 0.019	69/15=4.6
b) Modified track selection	0.984 ± 0.017	0.590 ± 0.021	55/15=3.7
c) Max. resonance correction	0.991 ± 0.016	0.605 ± 0.019	66/15=4.4
c) Min. resonance correction	1.014 ± 0.017	0.546 ± 0.019	75/15=5.0
d) Restricted fit range	1.011 ± 0.023	0.557 ± 0.024	67/10=6.7
e) Correlation function C	0.909 ± 0.017	0.580 ± 0.022	150/15=10.0

Table 4: *Results of the fits of Eq. 13 to several variations of C′(Q). The quoted errors are only statistical.*

The systematic error on the measured values of the parameters r and λ is evaluated in the same way as done for the three-dimensional analysis. The results of the various fits are summarized in Table 4.

The fit gives the following values for the parameters:

$$r = (1.002 \pm 0.016 \, (stat) \, {}^{+0.023}_{-0.096} \, (syst)) \, \text{fm} \quad , \quad \lambda = 0.574 \pm 0.019 \, (stat) \, {}^{+0.039}_{-0.036} \, (syst). \quad (14)$$

Since the percentage number of charged tracks which are pions is about 87%, one can estimate that the value of the λ parameter would be a factor of 1.32 larger in the case of a 100% pure pion sample.

The values of Eq. 14 are in agreement and replace the values previously published by the OPAL Collaboration, see ref. [2].

8   Conclusions

Using 4.3 million hadronic events from Z^0 decays, the Bose-Einstein correlation function for two identical charged bosons, mainly $\pi^\pm\pi^\pm$, is studied in the three components of the momentum difference, longitudinal and transverse ("out" and "side" components) with respect to the thrust direction, in the Longitudinally CoMoving System. The geometrical structure of the source is obtained from an extended Goldhaber fit of Eq. 9 to the Coulomb corrected BEC functions $C(Q_{t_{out}}, Q_{t_{side}}, Q_l)$ and $C'(Q_{t_{out}}, Q_{t_{side}}, Q_l)$. In all cases the longitudinal radius is significantly larger than the transverse radius.

The longitudinal and transverse radii of the emitting region are studied as a function of the two-jet resolution parameter y_{cut}. The analyses indicate that, as y_{cut} increases, $r_{t_{side}}$ increases slowly, r_l remains constant and that the ratio $r_l/r_{t_{side}}$ decreases. In the framework of the string model of ref. [13], the observed different values of the transverse and longitudinal correlation lengths are explained in terms of two different generation mechanisms of the longitudinal and transverse momentum components with respect to the string direction.

The fit of Eq. 9 to $C'(Q_{t_{out}}, Q_{t_{side}}, Q_l)$, in the case of two-jet events selected with $y_{cut} = 0.04$, yields the parameter values given in (12), in particular $r_l/r_{t_{side}} = 1.222 \pm 0.027 \, (stat) \, {}^{+0.075}_{-0.012}$ (syst). The corresponding value for the inclusive sample is $r_l/r_{t_{side}} = 1.194$, with similar uncer-

tainties.

The inclusive sample of events is also analysed in terms of the one-dimensional correlation function C'(Q). The fit gives the parameter values $r = (1.002 \pm 0.016 \ (stat) \ ^{+0.023}_{-0.096} \ (syst))$ fm and $\lambda = 0.574 \pm 0.019 \ (stat) \ ^{+0.039}_{-0.036} \ (syst)$.

In conclusion, the present analysis shows that the emitting source of two identical pions, measured in e^+e^- interactions at energies close to the Z^0 peak, is elongated. In particular, as computed in the LCMS, the emitting source for two identical pions has global dimensions of about 1 fm, but with the longitudinal dimension about 20% larger than the transverse dimension.

Acknowledgements

References

[1] See for example E. A. De Wolf; *Bose-Einstein Correlations* in Proc. XXVII Int. Conf. on High Energy Physics, Glasgow 20-27 July 1994 (Eds. P. J. Bussey and I. J. Knowles), Inst. of Phys. Publ., 1995, p. 1281;
G. Alexander and I. Cohen; *Measure of π's and Λ's emitter radius via Bose-Einstein and Fermi-Dirac statistics* in Proc. Int. Conf. on Hadron Structure, Stara Lesna, Slovakia, 7-13 September 1998 (Eds. D. Bruncko and P. Strizenec) p. 328.

[2] OPAL Coll., G. Alexander *et al.*, Z. Phys. C72 (1996) 389.

[3] ALEPH Coll., D. Decamp *et al.*, Z. Phys. C54 (1992) 75;
DELPHI Coll., P. Abreu *et al.*, Phys. Lett. B286 (1992) 201.

[4] H1 Coll., C. Adloff *et al.*, Z. Phys. C75 (1997) 437.

[5] ABCDHW Coll., A. Breakstone *et al.*, Phys. Lett. B162 (1985) 400;
UA1 Coll., C. Albajar *et al.*, Phys. Lett. B226 (1989) 410;
E735 Coll., T. Alexopoulos *et al.*, Phys. Rev. D48 (1993) 1931.

[6] EHS/NA22 Coll., N.M. Agababian *et al.*, Z. Phys. C71 (1996) 405;
EHS/NA22 Coll., N.M. Agababian *et al.*, Phys. Lett. B422 (1998) 359.

[7] NA35 Coll., T. Alber *et al.*, Z. Phys. C66 (1995) 77;
NA44 Coll., I.G. Bearden *et al.*, Phys. Rev. C58 (1998) 1656.

[8] ALEPH Coll., D. Buskulic *et al.*, Z. Phys. C64 (1994) 361;
DELPHI Coll., P. Abreu *et al.*, Phys. Lett. B323 (1994) 242;
OPAL Coll., R. Akers *et al.*, Z. Phys. C67 (1995) 389.

[9] DELPHI Coll., P. Abreu *et al.*, Phys. Lett. B379 (1996) 330;
OPAL Coll., G. Abbiendi *et al.*, CERN EP-99/163, submitted to Eur. Phys. Jou. C.

[10] DELPHI Coll., P. Abreu *et al.*, Phys. Lett. B401 (1997) 181;
OPAL Coll., G. Abbiendi *et al.*, Eur. Phys. Jou. C8 (1999) 559.

[11] DELPHI Coll., P. Abreu *et al.*, Phys. Lett. B355 (1995) 415;
OPAL Coll., K. Ackerstaff *et al.*, Eur. Phys. Jou. C5 (1998) 239.

[12] U. Heinz *et al.*, Phys. Lett. B382 (1996) 181;
U. Heinz; *Hanbury-Brown/Twiss interferometry for relativistic heavy ion collisions: theoretical aspects*, nucl-th/9609029;
K. Geiger, J. Ellis, U. Heinz and U.A. Wiedemann; *Bose-Einstein Correlations in a space-time approach to e^+e^- annihilation into hadrons*, hep-ph/9811270.

[13] B. Andersson and M. Ringner, Nucl. Phys. B513 (1998) 627; Phys. Lett. B421 (1998) 283.

[14] TASSO Coll., M. Althoff *et al.*, Z. Phys. C30 (1986) 355.

[15] L3 Coll., M. Acciarri *et al.*, Phys. Lett. B458/4 (1999) 517.

[16] OPAL Collaboration, K. Ahmet et al., Nucl. Instr. and Methods A305 (1991) 275; P.P. Allport et al., Nucl. Instr. and Methods A324 (1993) 34; Nucl. Instr. and Methods A346 (1994) 476.

[17] B.E. Anderson et al., IEEE Transactions on Nuclear Science 41 (1994) 845.

[18] S. Catani *et al.*, Phys. Lett. B269 (1991) 432.

[19] T. Csörgö and S. Pratt, in Proc. of the Workshop on Relativistic Heavy Ion Physics at Present and Future Accelerators, Budapest, KFKI-1991-28/A 14-21, p. 75.

[20] S. Chapman, P. Scotto and U. Heinz, Phys. Rev. Lett. 74 (1995) 4400.

[21] M. Gyulassy *et al.*, Phys. Rev. C20 (1979) 2267.

[22] T. Sjöstrand, Comp. Phys. Comm. 39 (1986) 347; T. Sjöstrand and M Bentgtsson, Comp. Phys. Comm. 43 (1987) 367; Comp. Phys. Comm. 82 (1994) 74.

[23] I.G. Knowles and G.D. Lafferty, J. Phys. G23 (1997) 731.

[24] G. Goldhaber, S. Goldhaber, W. Lee and A. Pais, Phys. Rev. Lett. 3 (1959) 181.